PB 161594

NBS

Technical Note 93

AN EXPERIMENTAL STUDY OF BETA DECAY USING THE RADIATIONS FROM ORIENTED NUCLEI

U. S. DEPARTMENT OF COMMERCE
NATIONAL BUREAU OF STANDARDS

THE NATIONAL BUREAU OF STANDARDS

Functions and Activities

The functions of the National Bureau of Standards are set forth in the Act of Congress, March 3, 1901, as amended by Congress in Public Law 619, 1950. These include the development and maintenance of the national standards of measurement and the provision of means and methods for making measurements consistent with these standards; the determination of physical constants and properties of materials; the development of methods and instruments for testing materials, devices, and structures; advisory services to government agencies on scientific and technical problems; invention and development of devices to serve special needs of the Government; and the development of standard practices, codes, and specifications. The work includes basic and applied research, development, engineering, instrumentation, testing, evaluation, calibration services, and various consultation and information services. Research projects are also performed for other government agencies when the work relates to and supplements the basic program of the Bureau or when the Bureau's unique competence is required. The scope of activities is suggested by the listing of divisions and sections on the inside of the back cover.

Publications

The results of the Bureau's research are published either in the Bureau's own series of publications or in the journals of professional and scientific societies. The Bureau itself publishes three periodicals available from the Government Printing Office: The Journal of Research, published in four separate sections, presents complete scientific and technical papers; the Technical News Bulletin presents summary and preliminary reports on work in progress; and Basic Radio Propagation Predictions provides data for determining the best frequencies to use for radio communication throughout the world. There are also five series of nonperiodical publications. Monographs, Applied Mathematics Series, Handbooks, Miscellaneous Publications, and Technical Notes.

A complete listing of the Bureau's publications can be found in National Bureau of Standards Circular 460, Publications of the National Bureau of Standards, 1901 to June 1947 ($1.25), and the Supplement to National Bureau of Standards Circular 460, July 1947 to June 1957 ($1.50), and Miscellaneous Publication 240, July 1957 to June 1960 (Includes Titles of Papers Published in Outside Journals 1950 to 1959) ($2.50), available from the Superintendent of Documents, Government Printing Office, Washington 25, D. C.

NATIONAL BUREAU OF STANDARDS

Technical Note

93

AUGUST 1961

AN EXPERIMENTAL STUDY OF BETA DECAY USING THE RADIATIONS FROM ORIENTED NUCLEI

Dale D. Hoppes

NBS Technical Notes are designed to supplement the Bureau's regular publications program. They provide a means for making available scientific data that are of transient or limited interest. Technical Notes may be listed or referred to in the open literature. They are for sale by the Office of Technical Services, U. S. Department of Commerce, Washington 25, D. C.

DISTRIBUTED BY

UNITED STATES DEPARTMENT OF COMMERCE

OFFICE OF TECHNICAL SERVICES

WASHINGTON 25, D. C.

Price $1.50

An Experimental Study of Beta Decay Using the Radiations from Oriented Nuclei*

Dale D. Hoppes

The angular distribution of electrons with respect to the nuclear spin direction is shown to furnish information about the relative contribution of the different operators in first-forbidden beta decay. An experimental determination of two coefficients in a Legendre polynomial expansion of this distribution function for a transition in the decay of cerium-141 is made by observing the radiations from both aligned and polarized nuclei. Together with calculations based on reliable shell model assumptions this information allows the determination of the relative contribution of the significant relativistic operator $\underset{\sim}{\alpha}$. The result $M(\underset{\sim}{\alpha})/M(\underset{\sim}{\sigma} \times \underset{\sim}{r}) = -29.4 \pm 1.5$ is compared with some general estimates of this quantity.

1. Introduction

The theory of beta decay is now sufficiently formulated that one can use measurements of angular distributions of the particles emitted

---

*This article was composed for the fulfillment of the publication requirement for the degree of Ph.D. in the School of Arts and Sciences of the Catholic University of America, Washington, D. C.

to obtain information about the initial and final nuclear states involved in the transition. In the present experiment the distribution of emitted electrons with respect to the nuclear spin direction is measured for a first-forbidden transition occurring in the decay of Ce^{141}. Sufficient information is obtained from subsidiary experiments and calculations to permit a determination of a reduced nuclear matrix element ratio which is sensitive to the radial nuclear wave functions and the composition of the nuclear potential.

In part 1.1 of the introduction the pertinent beta-decay formulae and approximations are discussed, while in part 1.2 the information necessary for a calculation of the nuclear orientation of Ce^{141} is presented. Previous experimental results on the decay of Ce^{141} are given in part 1.3.

1.1. Determination of the Reduced Nuclear Matrix Elements in First Forbidden Beta Decay [1,2,3]

In order to write the interaction Hamiltonian for use in a perturbation theory development of the beta-decay transition probability one must take selected products of the components of the spinor wave functions of the two nucleons and two leptons that are involved such that the result is relativistically invariant. It has been shown that if one forms a four-dimensional polar vector $(\underset{\sim}{\alpha}, 1)$ and axial vector $(\underset{\sim}{\sigma}, \gamma_5)$ from four-by-four Dirac matrices and then contracts the result of operating separately in the nucleon and lepton spaces with each of these operators, the essential interaction is established. The transformation of one nucleon into another is indicated by an i-spin

operator, while the non-conservation of parity can be completely described by writing $(1 + \gamma_5)$ times the operator in the lepton part. One sees that there are two types of operators present; $\underset{\sim}{\alpha}$ and γ_5 connect components of the nucleon wave functions which give terms of the order $(v/c)_{\text{nucleon}} \approx 1/10$ compared with the operators 1 and $\underset{\sim}{\sigma}$. The latter give the so-called allowed transitions in which the parity of the initial and final nuclear states is the same.

In order to see how other operators comparable to the $\underset{\sim}{\alpha}$ and γ_5 arise, one considers the leptons as free particles and makes a multipole expansion of the resulting plane wave, $e^{-i(\underset{\sim}{p}+\underset{\sim}{q})\cdot\underset{\sim}{r}}$, where $\underset{\sim}{p}$ and $\underset{\sim}{q}$ are the momentum of the electron and the neutrino, respectively. This yields a series of terms $\propto \sum_{\ell=0}^{\infty} \sum_{m=-\ell}^{\ell} \sum_{k=0}^{\ell} (pr)^{\ell-k} (qr)^{k} Y_{\ell m}(\theta,\varphi)$ where $Y_{\ell m}(\theta,\varphi)$ is a spherical harmonic. Since $p < 2$, $q < 2$, and $r < R$, the nuclear radius, ($R \approx 0.02$ in relativistic units), it is seen that the order of magnitude of succeeding terms will be $\approx (.04)^2$, since the Hamiltonian appears squared in the transition probability. Thus the leading term will be 1 or $\underset{\sim}{\sigma}$, while the next order terms for these operators are $\underset{\sim}{r}$ and $\underset{\sim}{\sigma r}$, respectively. The latter is separated into $\underset{\sim}{\sigma}\cdot\underset{\sim}{r}$, $\underset{\sim}{\sigma} \times \underset{\sim}{r}$, and B_{ij}, with respective tensor rank 0, 1, and 2. The leading term in the expansion for $\underset{\sim}{\alpha}$, or for γ_5, will be of the same order of magnitude as the second terms for the other operators and has the same requirement of a parity difference of the initial and final states. In table 1 the first forbidden operators are displayed, together with their tensor rank, selection rules, and a diagrammatic representation of the angular momentum, L, carried away by the leptons. The meaning of $\Delta(J_i J_f L)$ is

that the three numbers must be possible lengths of the sides of a triangle, possibly of zero area. The orbital angular momentum may be carried away by either the electron or the neutrino; also the wave function of the electron for a given total angular momentum will contain both $(\ell+1/2)$ and $(\ell-1/2)$ contributions of comparable magnitude, since $v/c \approx 1$ for the higher energy electrons. Thus an operator may have matrix elements between several lepton states.

In order to write general expressions for any angular relation that may be possible, one most wisely expresses the operators in spherical tensor form and proceeds by a density matrix method [4] that allows separation of angular and non-angular parts for each particle involved. This procedure makes it possible to easily sum over quantities that are not observable and obtain expressions which clearly display the origin of the remaining observables. As a pertinent example, let us consider the correlation of the direction of electron emission with respect to the nuclear spin axis [5,6,7]:

$$W(\underline{p},\underline{J}) = \sum_k (-1)^{k+L+L'} \overline{f}_k(J) F_k(L,L',J_f,J) b_k(L,L') P_k(\hat{p}\cdot\hat{J})$$

Here we wish to specify the coefficients of the possible Legendre polynomials, $P_k(\hat{p}\cdot\hat{J})$, which have as an argument the cosine of the angle between $\hat{p}$, a unit vector in the direction of electron emission, and $\hat{J}$, a unit vector in the direction of the initial state nuclear spin. The degree to which the latter can be considered a unique direction in space is given by

$$\bar{f}_k(J) = \sum_M (-)^{J-M}(JMJ\text{-}M|JJkO)a_M$$

where M, the magnetic quantum number, is the projection of J on the z axis, $(JMJ\text{-}M|JJkO)$ is a vector coupling coefficient and a_M is the fraction of the nuclei with projection M. The entire dependence on the nuclear orientation is contained in these parameters, in which k is the highest power of M that is considered in any $\bar{f}_k$. The $F_k(L,L',J_fJ)$ is an established product of numerical factors and vector coupling coefficients involving not only the order k and initial nuclear spin J, but also the selection rules of the term in that the two operator tensor ranks L and L' and the final nuclear state spin J_f must satisfy certain triangle conditions imposed by the vector coupling coefficients. These triangle relations are $\Delta(kLL')$, $\Delta(kJ_fJ_i)$, $\Delta(LJ_fJ_i)$ and $\Delta(L'J_fJ_i)$; they tell us just what $b_k(L,L')$ occur in the coefficient of $P_k(p\cdot J)$ for a given transition. The $b_k(L,L')$ contain the meat of the problem: the products of all nuclear matrix elements of tensor rank L and L' times their associated energy-dependent lepton functions. The $b_0(LL')$'s, which from $\Delta(kLL')$ consist of only $b_0(00)$, $b_0(11)$, and $b_0(22)$, multiply the isotropic term P_0 and give the shape factor, which is the departure of the spectral shape from that of an allowed transition, for unoriented nuclei. In general the higher terms of a distribution or correlation function must be divided by this isotropic term as a step in the interpretation of an experimental angular distribution as a function of energy.

Let us now consider the beta distribution function as applied to a $7/2^- \rightarrow 5/2^+$ transition. From the triangle conditions this first forbidden transition cannot involve L = 0 operators and will give only terms up to k = 4. We will write instead of $\bar{f}_k$ the more familiar quantity $f_k = \binom{2k}{k}^{-1} J^{-k}\left[\frac{(2J+k+1)!}{(2k+1)(2J-k)!}\right]^{\frac{1}{2}} \bar{f}_k$. Then, subsituting the values of known quantities, we find:

$$W(\underline{p},\underline{J}) = 1 - \left[\frac{b_1(11) + 0.527\, b_1(12) + 0.0361\, b_1(22)}{b_0(11) + b_0(22)}\right] f_1 P_1(\hat{p}\cdot\hat{J})$$

$$+ \left[\frac{0.582\, b_2(11) + 0.927\, b_2(12) + .0243\, b_2(22)}{b_0(11) + b_0(22)}\right] f_2 P_2(\hat{p}\cdot\hat{J})$$

$$+ \left[\frac{2.358\, b_3(12) + 2.721\, b_3(22)}{b_0(11) + b_0(22)}\right] f_3 P_3(\hat{p}\cdot\hat{J}).$$

The anticipated P_4 term does not appear because of a hidden triangle condition in the coupling of the neutrino and electron angular momenta to give $b_4(22)$.

Table 2 gives the $b_k(LL')$'s as derived from Bincer [6]. Here we write the reduced nuclear matrix elements of Bincer in the form $M(i\underline{r})$, $M(\underline{\sigma}\times\underline{r})$, $M(\underline{\alpha})$, and $M(iB_{ij})$. They are multiplied by the appropriate coupling coefficient, C_V or C_A, which gives the inherent strength of the interactions. From the corresponding lepton matrix elements we get

multiplying terms evaluated completely for the neutrino and down to the radial wave functions for the electrons. The quantities p, E, and q are respectively the magnitude of the electron momentum, electron energy, and the neutrino energy, which we will measure in relativistic units in which $\hbar$, m_e, and c are set equal to unity. The electron radial functions are contained in the quantities $K_{\kappa\kappa'}$, and $M_{\kappa\kappa'}$, which are similar to those defined by Bincer [8], with $\kappa = -(j+\frac{1}{2})$ for $j = \ell+\frac{1}{2}$ and $\kappa = +(j+\frac{1}{2})$ for $j = \ell-\frac{1}{2}$. Here

$$K_{\kappa\kappa'} = \frac{1}{2p^2} R^{-[\ell(\kappa)+\ell(\kappa')]} \left\{ g_\kappa g_{\kappa'} e^{i[\Delta(\kappa)-\Delta(\kappa')]} \right.$$

$$\left. + S(-\kappa)S(-\kappa') f_{-\kappa} f_{-\kappa'} e^{i[\Delta(-\kappa)-\Delta(-\kappa')]} \right\}$$

$$M_{\kappa\kappa'} = \frac{1}{2p^2} R^{-[\ell(\kappa)+\ell(\kappa')]} \left\{ S(-\kappa') g_\kappa f_{-\kappa'} e^{i[\Delta(\kappa)-\Delta(-\kappa')]} \right.$$

$$\left. + S(-\kappa) f_{-\kappa} g_{\kappa'} e^{i[\Delta(-\kappa)-\Delta(\kappa')]} \right\}$$

The f's and g's are the radial functions as calculated by Bhalla and Rose [9]; however the phase is chosen to fit the definition of Bincer [8]. The quantities $\ell(\kappa)$, $\Delta(\kappa)$, and $S(\kappa)$ represent the orbital quantum number, the phase, and the sign, respectively, for a given κ.

An estimate of the size of terms and a hint to the type of information that they yield is obtained if we consider the lepton wave functions

as those due to a point charge, but evaluate them at the nuclear radius. Furthermore, we use an expansion in powers of $\xi = \alpha Z/2R \approx 10$, take $(\alpha Z)^2 \ll 1$, and then consider only the highest power of ξ that appears in each $b_k(L,L')$. $M(\underset{\sim}{\alpha})$ does not have a multiplying ξ although it is estimated to contribute the same as elements that do, therefore we include it in the tensor rank one combination $\xi[C_V M(i\underset{\sim}{r}) + C_A M(\underset{\sim}{\sigma}\times\underset{\sim}{r})] - C_V M(\underset{\sim}{\alpha})$, which is considered as a unit. This combination carries just the energy dependence of the allowed transitions. Using this approximation, we estimate the $b_k(LL')$'s in table 3, from which several rough conclusions can be drawn. The respective magnitudes of the P_1, P_2, and P_3 coefficients are of the order 1, 1/10, and 1/100, aside from the respective nuclear orientation parameters, which also are of descending magnitude. Thus the higher orders are more difficult to measure experimentally, but it is just these terms that are more informative. This is true because the group $\xi[C_V M(i\underset{\sim}{r}) + C_A M(\underset{\sim}{\sigma}\times\underset{\sim}{r})] - C_V M(\underset{\sim}{\alpha})$ dominates the $b_0(11)$ and $b_1(11)$ terms, where it appears squared, and the $b_1(12)$ interference term, making it difficult to detect the individual tensor rank one matrix elements. In the $b_2(11)$ term, however, the combination $C_A M(\underset{\sim}{\sigma}\times\underset{\sim}{r}) - 2C_V M(i\underset{\sim}{r})$ occurs in the leading subterm.

Also, without knowing the individual matrix elements one can directly solve for the ratio of tensor rank two to tensor rank one contribution from a measurement of the coefficient of the P_1 term. These arguments apply also to other experiments in which information about the nuclear orientation is deduced from correlations with a

following gamma ray, since exactly the same b_k's appear. Similar conclusions can be drawn about a tensor rank zero unit contributing to a $\Delta J = 0$ transition.

In the past there have been attempts to interpret a few spectral-shape [10,11] and β- γ-correlation [12,13] measurements in which the leading terms in the ξ expansion have been small because of cancellation in the multiplying nuclear matrix element combination or in which this combination is small compared to the B_{ij} element because some secondary quantum relation involving the nuclear states is violated. In some cases the nuclear matrix elements have been treated as adjustable parameters and approximations have been made on the basis of the anticipated size of the result, with a satisfactory fit to the experiment being taken as justification for the degree of approximation [14]. In some schemes of analysis the effect of the finite nuclear size on the electron wave functions has been partly incorporated in the nuclear matrix elements, leading to extra parameters for each which depend on the electron angular momentum [15,16]. In the current experiment we measure directly the energy dependent quantities N_1/N_0 and N_2/N_0 appearing in the simplified beta distribution function

$$\frac{W(\underset{\sim}{p},\underset{\sim}{J})}{N_0} \simeq 1 + \frac{N_1}{N_0}\frac{p}{E} f_1 P_1(\hat{p}\cdot\hat{J}) + \frac{N_2}{N_0}\frac{p^2}{E} f_2 P_2(\hat{p}\cdot\hat{J})$$

for the $\Delta J = 1$ transition from the ground state of Ce^{141} to the ground state of Pr^{141}. Since a relatively large P_2 term is found, the data are analyzed without the usual approximations, but with the assistance of well-defined calculations of $\frac{M(i\underset{\sim}{r})}{M(\underset{\sim}{\sigma}\times\underset{\sim}{r})}$ and $\frac{M(iB_{ij})}{M(\underset{\sim}{\sigma}\times\underset{\sim}{r})}$ for shell model angular wave functions. The result is a value for $\frac{M(\underset{\sim}{\alpha})}{M(\underset{\sim}{\sigma}\times\underset{\sim}{r})}$, which is directly dependent on the nuclear radial functions.

In order to obtain information about the lower energy transition to the first excited state of Pr^{141}, one must measure the angular distribution for those beta particles which are in time-coincidence with the subsequent gamma ray. This more complicated correlation between the beta momentum, nuclear spin direction, and the gamma momentum (hereafter β - J - γ correlation) [17,18] is considered here only in order to determine the contribution of the lower beta group to the overall distribution, and so will not be discussed in detail. For this $\Delta J = 0$ transition all six matrix elements can contribute; thus the present experiment alone allows only a conditional analysis on the basis of the roughest approximation unless the results of theoretical calculations are again used to eliminate some of the variables.

1.2. Nuclear Orientation

The familiar spin Hamiltonian [19] with effective $S = 1/2$ is applicable to Ce^{141} in neodymium ethyl sulfate at temperatures below 1° K. This is written below, with the origin of each term indicated:

$$\mathcal{H} = [g_{||}\beta H_z S_z + g_{\perp}\beta(H_x S_x + H_y S_y)]$$ - Magnetic interaction of the ion and an external magnetic field

$$+ D[S_z^2 - 1/3\ S(S+1)]$$ - Interaction of the ion with the crystalline field.

$$+ [A\ S_z J_z + B(S_x J_x + S_y J_y)]$$ - Magnetic interaction of the nucleus with the ion.

$$+ P[J_z^2 - 1/3\ J(J+1)]$$ - Interaction of the nuclear electric quadrupole with the crystalline electric field.

+ other terms - ion dipole-dipole interactions, direct interaction of the nuclear magnetic moment with the external magnetic field, etc.

Here the standard terminology is used, with the exception of J for the nuclear spin.

Ideally, the constants in the Hamiltonian would be determined directly for the particular nucleus-ion-crystal combination by a resonance measurement, but this has not been done for the present case. Therefore, we make use of the information presented in a paper by an Oxford group on the angular distribution and linear polarization of gamma rays from oriented Ce^{141} in neodymium ethyl sulfate [20]. They give the values $g_{||} = 3.9$, $g_{\perp} = 0.2$, $A = 0.108(\mu_N/I)cm^{-1}$ and $B = 0.002(\mu_N/I)cm^{-1}$, based on measurements in concentrated cerium ethyl sulfate [21] and theoretical calculations [22]. The A and B values may be somewhat in error as stated, since the value of mean cube ionic radius [23] has been recalculated [24] and found to be somewhat lower, but if one uses in the A and B expressions the magnetic moment of Ce^{141}

as derived from resonance measurements [25] (in a double nitrate crystal) evaluated on the basis of the old radius, no error results from this change. A recent calculation of these A and B expressions gives slightly different results [26], but the present experiment is evaluated on the basis of the first values in anticipation of a more direct measurement of the required g's and A and B for eventual use in an accurate spin Hamiltonian.

The second term in the spin Hamiltonian is zero for $S = 1/2$; the fourth and fifth terms can be shown negligible for the present circumstances.

The spin Hamiltonian is now taken to have the following simple form for a magnetic field along the c-axis:

$$\mathcal{H} = (0.000262\, H_z - 0.0396\, J_z)S_z \ ^{\circ}K.$$

The sign of A is that for μ_N negative, which would be the shell model prediction for Ce^{141}. This sign is established by the present experiment.

The use of this simple Hamiltonian can be tested by calculating the relative population of the magnetic substates, a_M, where $M = J_z$, as a function of temperature for zero external field. From these one can calculate the orientation parameter f_2 as a function of temperature and then attempt to fit the Oxford measurements of the variation in gamma-ray intensity with temperature to the function $1 + A_2 f_2 P_2(\cos\theta)$. The Oxford measurements show that the f_4 contribution should be small,

and subsequent experiments have given the relationship between the magnetic temperature derived from the magnetic susceptibility and the true absolute temperature. The fit is good (within the error limits of the experiment) for $A_2 = 0.337$. We thus use this expression for the gamma-ray distribution to relate the change in gamma-ray intensity to the parameter f_2 for our different experimental conditions. Furthermore, we use the simplified spin Hamiltonian with $H_z = 205$ gauss to calculate the orientation parameters [27]

$$f_1 = 1/J \sum M a_M$$

$$f_2 = 1/J^2[\sum M^2 a_M - 1/3\ J(J+1)]$$

$$f_3 = 1/J^3[\sum M^3 a_M - 1/5\ (3J^2+3J-1)\sum M a_M]$$

for $J = 7/2$. We then find the odd f's, which define the nuclear polarization, from the alignment parameter f_2 by means of these relations. This use of the gamma-ray measurements to predict the orientation parameters is quite important, since the temperature of a thin radioactive surface layer cannot be reliably inferred from a measurement of the bulk crystal magnetic susceptibility. Furthermore, the relationship between the susceptibility and absolute temperature has not yet been directly established for neodymium ethyl sulfate in a magnetic field.

1.3. Experimental Information on Ce^{141}

The present information on the decay of Ce^{141} is shown in figure 1. Several spectral shape measurements have been made, [28,29,30,31] with some disagreement on the endpoint energies, but with no reports of other than an "allowed" shape. In general, data taken in the region between 435 and 580 kev has been extrapolated and subtracted from the total spectrum to yield an "allowed" spectrum for the 435 kev transition, although the lower region is somewhat masked by conversion and Auger electrons. In two cases $\beta - \gamma$ coincidences were used to separate the inner beta branch [29,32], which was found to be "allowed" in shape in the higher energy region for which measurements were reported. These investigations are stressed because the present results indicate that for the 580 kev spectrum there should be some deviation from an"allowed" shape which might be observed in a careful measurement.

Both the cerium [25] and praseodymium [33,34] ground state spins and magnetic moments have been measured. The measured magnetic moment of the Ce^{141} must be revised, due to new values [26] calculated for the ionic radii involved in the nuclear paramagnetic resonance determination.

As mentioned in the previous section, a simultaneous measurement of the gamma angular distribution and linear polarization in a nuclear orientation experiment [20] gave the ratio of electric quadrupole to magnetic dipole amplitude in the gamma transition as 0.08 ± 0.02. This experiment also gives information on the contribution of different tensor rank operators in the inner beta transition, but this effect is obscured by the uncertainty in the gamma-multipole mixing ratio.

2. Experiment and Analysis

2.1. Experimental Design and Procedure [35,36,37]

The requirements for the counting of beta particles at low temperatures have been met successfully in a series of recent experiments [38,39]. Figure 2 shows a typical counting arrangement used in the present experiment. In the inner chamber of a glass dewar system a 12-gram single crystal of neodymium ethyl sulfate is supported by a thin-walled bakelite tube about 10 centimeters long. Electrons emitted from a spot of activity at the top of the crystal are detected by an anthracene scintillator one to five centimeters above. The light pulses from the detecting crystal are transmitted through the glass window into a selected, shaped, lucite light pipe about 4 feet long which terminates in a selected photomultiplier outside the dewar system. The output of the photomultiplier is amplified and analyzed into 100 pulse-height channels.

The gamma distribution is sampled by three 2" x 2" NaI counters, connected in parallel, lying in an equatorial plane with respect to the c-axis of the source crystal and spaced 3.5 inches from the activity. The 145-kev gamma ray is selected and counted directly and is also used, by means of a fast-slow coincidence arrangement, to trigger a 100-channel beta analyzer. This provides a separate measurement of the $\beta - \gamma - J$ correlation for the inner transition. In addition, another gamma counter is located in a polar position below the dewar system.

A polarizing field is supplied by a copper-wound, liquid-cooled solenoid which can be raised about the tail of the dewar system. The

field for the adiabatic demagnetization is supplied by a 23 kilogauss electromagnet. The dewar system and pumping manifolds are of conventional design and permit, with the use of an oil diffusion pump, helium bath temperatures below 1° K. Coils for the measurement of the bulk magnetic susceptibility of the paramagnetic crystal are wound on the outside wall of the experimental chamber. The sample is inserted through a tapered ground glass socket at the bottom of the chamber; this opening is filled with a plug carrying the sample and sealed in place by the same soap-glycerine mixture that holds the anthracene crystal in place. An optical system using reflections from the source crystal faces is used to check the position of the alignment axis.

The Ce^{141} used in these experiments was obtained from cerium oxide irradiated for 3 weeks in a flux of about 10^{13} neutrons/sec/cm^2. After a Ce^{143} impurity had decayed a chemical separation involving the selective precipitation of cerium and zirconium iodates and cerium hydroxide was performed to remove the Pr^{143} and Pa^{233} activities that remained. Spectra taken with scintillation spectrometers and a thick-lens beta-ray spectrometer confirmed the purity of the final Ce^{141} fraction. Neodymium ethyl sulfate was prepared by stirring together, in a large excess of water, di-ethyl sulfate and neodymium hydroxide and was then purified by successive recrystallization. The active crystals were prepared by touching the desired spot on a mounted inactive single crystal into a pool of about 10 drops of saturated neodymium ethyl sulfate solution containing about 1/2 millicurie of the separated Ce^{141}. After about one hour the contact was broken and the active area of the crystal

was trimmed with a scalpel to a disk of about 1/4 inch diameter. The resultant activity was about 10-50 μc, which was sufficient to give reasonable counting rates in the experimental geometry without excessive heating.

The crystal was then mounted in the apparatus, the dewars were slipped on, and the assembly was slowly cooled to the temperature of liquid nitrogen. At this point the helium space and experimental space were evacuated, helium gas was introduced and liquid helium then added. Pumping on the liquid helium reduced the temperature to about 1° K, at which time the assembly was placed in the large magnet and the 23,000 gauss field applied. After thermal equilibrium had been established the exchange gas was pumped out and the field removed. The temperature of the sample fell to about 0.02° K as indicated by the magnetic susceptibility and as predicted by previous measurements which also gave the relation between the susceptibility and the temperature.

In one series of runs the ratio N_2/N_0 was measured alone by observing the counting rates in each of the β channels and the γ peaks for about 15 minutes while the sample was aligned, then briefly admitting a small amount of helium gas into the experimental space to heat the sample so that a measurement of the isotropic radiations could be made for a corresponding length of time. The ratio of the counting rates "cold" and "warm", when properly corrected for attenuating effects, thus gives the ratio of the P_2 term to the isotropic term, for the particular angles at which the β and γ counts are taken. In this particular case the P_4 gamma-ray distribution term contribution is

negligible, both from the very small value of f_4 and from the relatively small contribution that the necessary quadrupole operator makes to the transition. The uncorrected cold-to-warm ratio was typically 1.06 for the upper beta channels and 0.968 for the equatorial gamma counters.

For this particular set of runs the gamma anisotropy did not correspond to that anticipated from the demagnetization conditions, indicating that local heating occurred or that the cerium was not all properly located in the crystalline lattice. Since only f_2, which is given correctly in either case by the gamma measurements, is desired, the attenuation is not important. In the polarization measurements, in which f_2 is determined from f_1 with the supposition of full crystal acceptance of the cerium ions, spot checks without field showed that indeed the gamma anisotropy was in agreement with the predicted temperature for the source on which the present data are based.

For the polarization experiments a field of 205 gauss was applied along the c-axis of the crystal. This resulted in an increase in the temperature of the sample and consequently a decrease in the orientation parameter f_2, but maximized the parameter f_1, as evidenced by the greatest cold-warm difference in the beta counting rate. In this case, the rate of warm-up of the sample was greatly diminished, due to the increased specific heat of the neodymium ethyl sulfate in a magnetic field. Counting was continued for periods up to one hour before the sample was warmed and the normalizing counts taken. During this time the uncorrected beta-ray cold-to-warm intensity ratio was typically 1.30 for the field in the direction of the electron detector and 0.76 for the

opposite field. The uncorrected equatorial gamma ratio was about 0.975.

The data in this latter type experiment give twice the ratio of the $P_2(\hat{p}\cdot\hat{J})$ term to the isotropic term if the corrected quantities $(\frac{I_c}{I_w} - 1)$ for the two field directions are summed and twice the ratio of the $P_1(\hat{p}\cdot\hat{J})$ term to the isotropic if the difference is taken.

The above runs also give information on the $\beta - \gamma - J$ correlation [17] for the 435-kev transition in the present simplifying geometry in which the gamma rays are detected at right angles to the electron momentum-nuclear spin axis. This measurement is less accurate due to the reduced counting rate available in the coincidence system, but the difference in the uncorrected quantities $(\frac{I_c}{I_w} - 1)$ for the two field directions, plus 0.22, is still determined to about 10%, as measured by the standard deviation of 7 runs. The sum of these two ratios, which measures the P_2 term, is slightly negative, but zero within the accuracy of measurement.

2.2. Experimental Corrections and Evaluation of Data

Since the coefficients N_0, N_1, and N_2 contain energy dependences which in theory are characteristic of the individual matrix element combinations, a measurement of N_1/N_0 and N_2/N_0 as a function of energy is desirable. Usually the P_1 coefficient, like the spectral shape factor N_0 itself, is dominated by a combination of matrix elements with a common p/E energy dependence. For the P_2 coefficient the characteristic energy dependence is expected to be p^2/E unless there is cancellation among the matrix elements or unless the B_{ij} element is dominant.

In order to make a best determination of the energy dependences several corrections to the data are necessary. We will consider these in turn, together with the limitations on the accuracy imposed by each.

(1) Background

In this respect Ce^{141} is quite good compared to other materials which have been used for low temperature beta spectroscopy [38,39], for in the present case internal conversion electrons and electrons from Compton scattering of the gamma ray occur only in the lower-energy region of the beta distributions, where electron scattering prevents analysis. Background due to gamma rays and cosmic rays striking the beta scintillator are minimized by the small crystal size; these and other contributions from phototube and amplifier noise and electrons scattered from the walls were shown to be quite negligible by measurements made with the detector just barely shielded from the direct beta radiation from the source.

For the gamma detectors the background was small and reproducible; it was subtracted as the first step in the analysis of the gamma distribution.

(2) Solid angle corrections

For the alignment (no magnetic field) experiments in which coincidences were not recorded, the source-beta detector distance was 2.5 centimeters. In order to correct for the fact that angles other than the assumed 0 or π were involved, a multiplicative correction to the P_2 term of 1.025 was applied, following the calculations of Rose [40]. For the polarization runs the source-beta detector distance was 1 cm

with a source radius of 0.125 inches and a detector radius of 0.219 inches - a geometry too poor to permit the use of available correction formulae. A Monte Carlo computer calculation for this geometry gave the attenuation coefficient 0.925 for the P_1 term and 0.788 for the P_2 term. Application of the Rose formula to the gamma detectors gave attenuation coefficients of 0.944 to 0.988, depending on the location. All these multiplicative corrections (the reciprocals of the attenuation coefficients) were applied in a final step.

(3) Electron backscattering [41,42]

The backing for the beta source is a crystal of $Nd(C_2H_5SO_4)_3 \cdot 9H_2O$, whose electron backscattering properties have not been investigated directly. Moreover, there is very little quantitative information on the angular and energy distribution of electrons backscattered from any material in the region of 100 to 600 kev. In view of this lack of information, the following scheme of analysis was adopted:

a) From the available date [43,44,45,46] a composite spectrum of backscattered electrons as a function of fraction of the incident energy for all incident angles scattered into the detector in our geometry was constructed.

b) The data of Bothe [43] and Seliger [47] was used to normalize the above spectrum to the total relative backscatter expected from a crystal of the present composition.

c) Theoretical allowed spectra for the two beta groups were constructed, and divided into energy bins. The backscatter contribution of each energy bin in all other bins was calculated for each spectrum

from the data of part (b).

d) Only the upper part of each spectrum was considered in the final analysis, such that the backscattered contribution was less than 5% of the total in the lowest bin.

e) In the case of the P_1 term, the correction was applied to each β channel by multiplying each $(\frac{I_c}{I_w} - 1)$ by the quantity $\frac{I + b}{I - b/2}$ where b is the fractional contribution of the backscattered electrons to that channel. For the P_2 term the correction used was of the form $(1 + b)$.

(4) Resolution

In this particular set of runs the resolution, $(\frac{\Delta E}{E})$ at 1/2 the peak maximum, of the beta detector was 30% for 624 Cs^{137} conversion electrons. This comparatively poor resolution meant that the counts collected in a given channel of the pulse height analyzer at a nominal energy were due to electrons of a range of energies.

This correction was treated quite like that of the backscattered electrons. Each of the theoretical and backscatter spectra was divided into bins, and the area of each bin was apportioned over neighboring bins according to a Gaussian distribution of the correct width. The change of resolution with energy and the absence of a low energy tail significant for the type and range of spectra analyzed was checked by measuring the response of the system to monoenergetic electrons from the exit port of a beta-spectrometer. Thus, in the end, the upper part of the experimental spectrum was reproduced from the synthesis of the two theoretical spectra and the backscatter spectrum of each. Each energy bin was assigned a mean energy for each of the four components,

based on an intensity-weighted average of original bins from which the contributions came. The effect of contributions from the lower spectrum were considered in evaluating the upper spectrum results.

(5) Thick-source scattering [48]

For angular correlations involving electrons, one usually chooses to make the source as thin as possible. In the present case there is the conflicting requirement that one must also be certain that the Ce^{141} ions are included in the crystalline lattice, especially if one is to infer the f_1 orientation parameter from the f_2. With the specific activity available it was not possible to prepare satisfactory sources by dissolving some of the mother crystal and allowing it to recrystallize with a small amount of active solution, as has been done with other materials [39]. Therefore, a crystalline layer of the order of 1/10 millimeter thick was grown on the mother crystal, the thickness being somewhat uncertain because it was not known to what extent the base crystal was dissolved. An attempt to determine the thickness by slowly removing the active material with a microtome did not prove successful, mostly due to difficulty in holding the crystal securely.

Calculations such as those suggested by Frankel [48] indicated that for our approximate thickness scattering should become quite important for the lower part of the spectrum. For this reason also only the upper part of the spectrum is considered, where for Co^{60} grown crystalline layers and "thin" sources gave the same polarization results, namely the maximum predicted by theory.

(6) Analyzer dead time losses

Although the beta pulse height analyzer does not distort the spectrum as the counting losses increase, the cold to warm intensity ratio is in error by 5 to 15%. The losses were determined by finding the dead-time of each channel and integrating over all channels; this correction was applied to all data before ratios were taken.

(7) Corrections to the $\beta - \gamma - J$ coincidence data

In general, the corrections were as for the non-coincidence data, with the difference that accidental coincidences were subtracted from all data. These coincidences were obtained by duplicating the counting rates of the real experiment, but with the gamma detectors receiving radiation only from a separate source of Ce^{141}. The ratio of true coincidences to accidental coincidences was in all cases greater than 10.

When all the above corrections are applied one obtains a value of $-N_1/N_0$ as a function of beta channel number as shown for the 580-kev beta transition in figure (3), where the nominal energies for the first and last points shown are 392 and 566 kev respectively. The error in the early channels stems mainly from uncertainty in the inner spectrum contribution and backscattering corrections and in the effect of thick source scattering, while in the upper channels the uncertainty arises mostly from counting statistics.

The energy dependence over this restricted region is very slight compared to the realistic limits of error shown on the points. For this reason the above values are averaged to a value of -1.11 ± 0.10

for N_1/N_0 at an average energy of $1.85\ m_o c^2 = 434$ kev. The above limits included a nominal 5% uncertainty in f_1 in addition to the other sources already mentioned.

Similar arguments about the lack of visible energy dependence within the error of measurement leads to the averaging of the alignment and polarization data to give an average value of $+0.36 \pm 0.10$ for N_2/N_0. This value, while derived from a rather small experimental change compared to that due to the P_1 term, is still almost an order of magnitude larger than anticipated in the ξ approximation and provides the basis for the extended analysis in the next section.

The $\beta - \gamma - J$ runs represent a total of three hours of counting with the nuclei oriented. This cumulated data, after correction for accidental coincidences and the effect of the pure gamma distribution term, yields for an average over the upper channels the experimental quantity $1/2[\frac{I(0) - I(\pi)}{I_{warm}}] = +0.113 \pm 0.015$. The angle of 0 or π is that between p and J. When corrected as described above and evaluated for an average energy of $1.68\ m_o c^2$ with $f_1 = -0.373$, this value gives -0.42 ± 0.06 for N_1/N_0 in the distribution function $1 + N_1/N_0\ p/E\ f_1 + N_2/N_0\ p^2/E\ f_2$ for the angles selected in the experiment. A similar treatment for $1/2[\frac{I(0) + I(\pi)}{I_{warm}}]$ yields a value for N_2/N_0 of -0.13 ± 0.15.

2.3. Interpretation of data and conclusions

In order to illustrate the magnitude of terms and indicate the type of information that can be obtained from an approximate analysis, we first consider the beta angular distribution for the 580-kev transition

in an approximation using the highest power of ξ multiplying each matrix element combination in each $b_k(LL')$. Using this procedure one makes no assumptions about the relative size of the matrix elements, but makes considerable error in the estimation of numerical coefficients. The approximation does assume that the tensor rank one operator matrix element combination $\xi[C_A M(\underset{\sim}{\sigma}\times\underset{\sim}{r}) + C_V M(i\underset{\sim}{r})] - C_V M(\underset{\sim}{\alpha})$ is not appreciably less than its largest term.

Comparing the result of this approximation to the experimental N_1/N_0, it is seen that the ratio of the tensor rank two matrix element to the grouping of tensor rank one matrix elements is as shown in figure (4). The alternate choice for this ratio in the solution of a quadratic expression would lead to a predominance of $M(iB_{ij})$ incompatible with the spectral shape. A similar comparison of the approximation for the $b_2(LL')$'s with the experimental N_2/N_0 gives a value for the ratio of $C_A M(\underset{\sim}{\sigma}\times\underset{\sim}{r}) - 2C_V M(i\underset{\sim}{r})$ to $\xi[C_A M(\underset{\sim}{\sigma}\times\underset{\sim}{r}) + C_V M(i\underset{\sim}{r})] - C_V M(\underset{\sim}{\alpha})$ as shown in figure (5), where the results of figure (4) are also used.

The effectiveness of such an approximation for a given case is necessarily checked by considering the importance of higher terms in the ξ expansion. When all terms down through order zero in ξ are considered, the usefulness of the grouping of tensor rank one elements is lost, and one must consider the problem at least as one in the ratio of three matrix elements to a fourth. The present experiment then does not yield sufficient equations to determine the three unknowns, unless one uses the limits on the energy dependence from the N_1/N_0 term or N_0 (spectral shape measurement) as a third equation. Such a technique

does not lead to well-defined matrix element ratios in the present case, but does show that for possible values of the parameters the neglected terms in the ξ expansion may be larger than those used in the first approximation.

We now consider a method of analysis almost specific for Ce^{141}. It is based on the fact that with well-defined shell model angular wave functions one can calculate precisely the ratios of any two of the set $M(i\underset{\sim}{r})$, $M(iB_{ij})$, and $M(\underset{\sim}{\sigma}\times\underset{\sim}{r})$ to the third [49,50], with no assumptions about the nuclear radial functions. The ratio of the matrix element of $M(\underset{\sim}{\alpha})$ to any of the set, however, depends directly on the radial functions.

The correctness of our evaluation procedure depends strongly on the firmness with which the shell model [51] predictions for the initial and final state wave functions can be established. The cerium ground state consists of 58 protons and 83 neutrons, and is with some certainty a pure $2f_{7/2}$ neutron state. The praseodymium ground state with 59 protons and 82 neutrons has most simply the proton configuration $(1g_{7/2})^8(2d_{5/2})^1$, as would be indicated by the $_{55}Cs^{137}_{82}$ ground state configuration of $(g_{7/2})^5(d_{5/2})^0$, but other configurations are not ruled out. Recent discussions [52,53], have pointed out that the configuration $(g_{7/2})^6(d_{5/2})^3$ must be considered and that $(g_{7/2})^4(d_{5/2})^5$ may also contribute. Higher seniority configurations can be expected to be much less important. However, in the calculation of the ratios $M(i\underset{\sim}{r})/M(\underset{\sim}{\sigma}\times\underset{\sim}{r})$ and $M(iB_{ij})/M(\underset{\sim}{\sigma}\times\underset{\sim}{r})$ all the first mentioned configurations give exactly the same value, and the higher seniority configurations give zero contribution.

In order to calculate the nuclear matrix elements, let us define the operators in their spherical tensor form, using the terminology of Edmonds. These definitions are the equivalent of those of Morita and Morita [7] and Bincer [6]. We include an $\underline{i}$ with certain operators so that all ratios of matrix elements will be real. We define the spherical tensor

$$T_{J\ell}^{M}(B,\underline{r}) = \sum_{m_1 m_2} i^{\ell} B_{km_1} \mathcal{Y}_{\ell m_2}(\underline{r})(km_1 \ell m_2 | k\ell JM)$$

in which $\mathcal{Y}_{\ell m_2}(\underline{r})$ is a solid spherical harmonic, $(km_1 \ell m_2 | k\ell JM)$ is a vector coupling coefficient, and B_{km_1} is a spherical tensor characteristic of each operator. We also make use of the canonical transformation in the case of the operator $\underline{\alpha}$, in order to transform it into a form that can be used with the non-relativistic nuclear wave functions. In table 4 we give each matrix element with its equal in tensor operator form.

We next use the appropriate formulae of Edmonds [50], chapter 7, for operators in a coupled scheme, and find the reduced matrix elements of the individual operators as shown in his chapter 5. The results of these calculations are:

$$\frac{M(i\underline{r})}{M(\underline{\sigma}\times\underline{r})} = -1$$

$$\frac{M(iB_{ij})}{M(\underline{\sigma}\times\underline{r})} = -3\sqrt{2/5}$$

$$\frac{M(\underset{\sim}{\alpha})}{M(\underset{\sim}{\sigma}\times\underset{\sim}{r})} = -\frac{1}{M}\,\frac{\int r^2 U_f^*(r)\left(\frac{d}{dr}+\frac{4}{r}\right)U_i(r)\,dr}{\int r^3 U_f^*(r)U_i(r)\,dr}$$

Thus the first two ratios are pure numbers while the third depends on the radial functions of the initial and final state and their derivatives. For this reason the experimental determination of this third ratio is deemed most interesting and we use the first two ratios, together with the value $C_A = -1.21\ C_V$ from the decay of the neutron [54], to calculate theoretical values for our <u>two</u> experimental results as a function of $M(\underset{\sim}{\alpha})/M(\underset{\sim}{\sigma}\times\underset{\sim}{r})$.

One must next consider the best values to use for the electron radial wave functions. These would be solutions for the Dirac equation for the nuclear charge distribution, evaluated at a radial distance corresponding to the mean radius of the decaying nucleon in the correct shell. There are available calculations by Bhalla and Rose [9] in which a spherical charge distribution of radius $1.2A^{1/3}\ 10^{-13}$ centimeters is assumed; however, the functions are only evaluated at the same radius. We have followed the scheme of the above authors in calculating, for an average energy of $1.85\ m_o c^2$, all necessary electron radial functions for that value of the radius and for a radius 8% greater. It is felt that the larger radius is probably more representative of the point of interaction, while not seriously changing the general radial solutions. These values were then used to calculate the necessary $b_k(LL')$'s as a function of $M(\underset{\sim}{\alpha})/M(\underset{\sim}{\sigma}\times\underset{\sim}{r})$, and thus to form the quantities N_1/N_0 and N_2/N_0 which are compared with experiment in figure (6).

Taking the region where there is a common solution to represent the possible values of $\frac{C_V M(\underset{\sim}{\alpha})}{C_A M(\underset{\sim}{\sigma} x \underset{\sim}{r})}$, we arrive at the values shown in table 5, where the approximate solution in which the ξ expansion is considered in its three highest powers, but with the neglect of $(\alpha Z)^2$ terms, is shown by way of contrast. While the two more precise calculations give very similar values for $M(\underset{\sim}{\alpha})/M(\underset{\sim}{\sigma} x \underset{\sim}{r})$ it is seen from figure 7 that it is somewhat accidental that the agreement is so close, since a slightly smaller radius would not give a solution at all, while the value would shift somewhat for a radius of $1.4A^{1/3}\ 10^{-13}$ cm. Moreover, the shape correction factor is dependent on this choice of radius as well as the value of $M(\underset{\sim}{\alpha})/M(\underset{\sim}{\sigma} x \underset{\sim}{r})$. Calculations of the shape factor using the radial wave functions of Bhalla and Rose [9], but using different explicit radial values in forming the K's and M's of Bincer [6] indicate that higher values of the nuclear radius and of the ratio of $M(\underset{\sim}{\alpha})/M(\underset{\sim}{\sigma} x \underset{\sim}{r})$ give a more nearly allowed shape. However, more careful execution of this rather difficult shape measurement would be of considerable interest.

3. Discussion

The experimental value of approximately -29 for the ratio $M(\underset{\sim}{\alpha})/M(\underset{\sim}{\sigma} x \underset{\sim}{r})$ is to be compared with the values for $\frac{-1}{M} \frac{\int r^2 U_f^*(r)(\frac{d}{dr} + \frac{4}{r})U_i(r)dr}{\int r^3 U_f^*(r)U_i(r)dr}$ for possible initial and final state radial functions. These calculations are beyond the scope of this discussion, but would appear to be of considerable theoretical interest.

The relative contribution of $\underset{\sim}{\alpha}$ and γ_5 to the first forbidden transitions has been discussed by Pursey [55], Ahrens and Feenberg [56], and Rose and Osborne [49]. Pursey adopts the single particle model and a specific nuclear Hamiltonian containing short-range two-particle ordinary, charge exchange, and spin-orbit forces. He then derives a relation between $M(\underset{\sim}{\alpha})$ and $M(i\underset{\sim}{r})$ by calculating the commutator of r (times the correct i-spin operators) with the complete nuclear Hamiltonian. By averaging over a spherical core plus one transforming particle and assuming particular potentials, he finds:

$$M(\underset{\sim}{\alpha}) = XM(i\underset{\sim}{r}), \text{ where}$$

$$X = (W_i - W_f) - (M_n - M_p) + \left(\frac{\alpha Z}{R}\right)$$

$$- 15A^{-4/3}(N-Z)(1-3A^{-2/3})$$

$$- 3(K_i - K_f)A^{-1/3}(1-3A^{-2/3}).$$

For the case at hand $X = +25$. The measured value for this quantity is $+29.4$.

Ahrens and Feenberg [56] use the commutator relation between r and the complete nuclear Hamiltonian to establish a relation between $M(\underset{\sim}{\alpha})$ and $M(i\underset{\sim}{r})$, but evaluate the necessary commutators with the Coulomb and specifically nuclear parts of the Hamiltonian without assuming a definite nuclear potential. There is an assumption that off-diagonal

terms in the matrix elements of H_C and $H_{nuclear}$ are small for both the initial and final states or that the nuclear beta decay matrix element is relatively small for states other than the specified initial and final ones. The specifically nuclear contribution is evaluated from the semi-empirical energy formula, with reference to the treatment of the nucleus as a degenerate gas of free particles to apportion the terms between potential and kinetic energy. Under the circumstances they find $M(\underset{\sim}{\alpha})/M(\underset{\sim}{ir}) = \frac{\alpha Z}{2R} A$, where $A = 1 + (W_0-2.5)A^{1/3}/Z$ for β^- emission. For Ce^{141}, this would give $M(\underset{\sim}{\alpha})/M(\underset{\sim}{ir}) \approx 12$ instead of the measured 29. Ahrens and Feenberg point out that if they make the assumption of only short range, two-particle nuclear interactions (equivalent in effect to the Hamiltonian of Pursey and contrary to their first evaluation), they would calculate $A \approx 2.4 + (W_0-2.5)A^{1/3}Z$. This would give a value of about 29 for Ce^{141}.

Rose and Osborne [49], in addition to deriving the ratio of radial integrals that we have calculated for $M(\underset{\sim}{\alpha})/M(\underset{\sim}{ir})$, also use a manipulation of the radial equations to convert the numerator into an integral of the product of the initial and final radial wave functions plus another integral involving the nuclear potential.

The latter integral is taken to have contributions from only Coulomb and spin-orbit terms. In general, they predict $M(\underset{\sim}{\alpha})/M(\underset{\sim}{ir}) \approx 12$ to 37 for the present circumstances. In their derivation they also make assumptions about the commutation properties of the nuclear potentials.

In all the above calculations the arguments are of a somewhat general nature, with a possibility of some variation in specific cases. For this reason other measurements of the relative contribution of the relativistic operators are important. One other ratio which has been measured and analyzed in a straight-forward manner is that of the ratio $M(\gamma_5)/M(i\underset{\sim}{\sigma}\cdot\underset{\sim}{r})$ in the $0^- \rightarrow 0^+$ transition of Pr^{144} [10,57]. Although there is some question as to the sign of the ratio, the absolute magnitude seems to be considerably lower than that which would be inferred from the present tensor rank one analogue.

4. Summary

In the present experiment, the use of the nuclear orientation technique permits a significant matrix element ratio measurement for a particularly interesting but otherwise rather inaccessible transition. While the experimental techniques are difficult and the final value of -29.4 for $M(\underset{\sim}{\alpha})/M(\underset{\sim}{\sigma}\times\underset{\sim}{r})$ may change by five to ten percent when the correct hyperfine constants are known, the accuracy is still sufficient to provide a good check for the general expression discussed in section 3, and to serve as a goal in the determination of radial shell model wave functions.

5. Acknowledgments

I wish to thank R. S. Kaeser for much of the cryogenic design and assistance with the experiments; Dr. R. W. Hayward for his assistance in the interpretation of the results; Dr. E. Ambler and Dr. R. P. Hudson for much advice on the nuclear orientation aspects of the problem and for the use of their equipment; and the members of the Radioactivity Section and the Cryogenic Physics Section who have assisted me in many ways.

I also wish to thank Dr. F. L. Talbott for directing this thesis and Dr. J. G. Brennan for advice on the theoretical aspects of the problem.

References

[1] E. J. Konopinski, Annual Reviews of Nuclear Science, edited by E. Segrè and L. I. Schiff (Annual Reviews, Inc., Palo Alto, Calif., 1959) 9, p. 99.

[2] M. Deutsch and O. Kofoed-Hansen, Experimental Nuclear Physics, edited by E. Segrè (Wiley, New York, 1959) 3, p. 427.

[3] M. E. Rose, Handbook of Physics, edited by E. U. Condon and H. Odishaw (McGraw-Hill, New York, 1958) p. 9-90.

[4] S. Devons and L.J.B. Goldfarb, Encyclopedia of Physics, edited by S. Flügge (Springer-Verlag, Berlin, 1957) 42, p. 362.

[5] K. Alder, B. Stetch, and A. Winther, Phys. Rev. 107, 728 (1957).

[6] A. Bincer, Phys. Rev. 112, 244 (1958).

[7] M. Morita and R. S. Morita, Phys. Rev. 109, 2048 (1958).

[8] A. Bincer, Op. Cit., p. 248.

[9] C. P. Bhalla and M. E. Rose, ORNL-2954, Oct. 3, 1960 (unpublished).

[10] F. T. Porter and P. P. Day, Phys. Rev. 114, 1286 (1959).

[11] Bincer, Church, and Weneser, Phys. Rev. Letters 1, 95 (1958).

[12] G. Hartwig and H. Schopper, Phys. Rev. Letters 4, 293 (1960).

[13] R. M. Steffen, Phys. Rev. Letters 4, 290 (1960).

[14] T. Kotani, Phys. Rev. 114, 795 (1959).

[15] Z. Matumoto, Progr. Theoret. Phys. (Kyoto) 23, 643 (1960).

[16] T. Kotani and M. Ross, Progr. Theoret. Phys. (Kyoto) 20, 643 (1958).

[17] M. Morita and R. S. Morita, Phys. Rev. 110, 461 (1958).

[18] A. Z. Dolginov, Nuclear Phys. 7, 591 (1958).

[19] E. Ambler, Progress in Cryogenics, edited by K. Mendelsson, (Heywood, London, 1960) 2, p. 235.

[20] Cacho, Grace, Johnson, Knipper, Scurlock, and Taylor, Phil. Mag. 46, 1287 (1955). A private communication from C. E. Johnson to E. Ambler gives a revised gamma anisotropy versus temperature curve based on subsequent measurements relating the magnetic and absolute temperatures. [H. Meyer, Phil. Mag. 2, 521 (1957)].

[21] Bogle, Cooke, and Whitley, Proc. Phys. Soc. (London) A64, 931 (1951).

[22] R. J. Elliot and K. W. H. Stevens, Proc. Roy. Soc. A215, 437 (1952); A219, 387 (1953).

[23] B. Bleany, Proc. Phys. Soc. (London) A68, 937 (1955).

[24] B. R. Judd and I. P. K. Lindgren, Theory of Zeeman Effect in the Ground State, UCRL-9188, May 9, 1960 (unpublished).

[25] Kedzie, Abraham, and Jeffries, Phys. Rev. 108, 54 (1957).

[26] Haag, Johnson, Shirley, and Templeton, Phys. Rev. 121, 591 (1961).

[27] H. A. Tolhoek and J. A. M. Cox, Physica 19, 101 (1953).

[28] M. S. Freedman and D. W. Engelkemier, Phys. Rev. 79, 897 (1950).

[29] J. T. Jones and E. N. Jensen, Phys. Rev. 97, 1031 (1955).

[30] Joshi, Subba Rao, and Thosar, Il Nuovo Cimento 9, 601 (1958).

[31] E. Kondiah, Arkiv für Fysik 4, 81 (1951).

[32] R. L. Robinson and L. M. Langer, Phys. Rev. 109, 1255 (1957).

[33] J. E. Mack, Rev. Modern Phys. 22, 64 (1950).

[34] H. Lew, Phys. Rev. 91, 619 (1953).

[35] See, for example, Chapters 5, 7, and 9, Beta and Gamma Ray Spectroscopy, edited by K. Siegbahn (Interscience, New York, 1955).

[36] R. W. Hayward and D. D. Hoppes, IRE Trans. on Nuclear Science (IRE, New York, 1958) NS5, No. 3.

[37] H. Postma, Thesis, Groningen (1960).

[38] Wu, Ambler, Hayward, Hoppes, and Hudson, Phys. Rev. 105, 1413 (1957); Phys. Rev. 106, 1361 (1957).

[39] Ambler, Hayward, Hoppes, and Hudson, Phys. Rev. 108, 503 (1957); Phys. Rev. 110, 787 (1958).

[40] M. E. Rose, Phys. Rev. 91, 610 (1953).

[41] R. D. Birkhoff, Encyclopedia of Physics, edited by S. Flügge (Springer-Verlag, Berlin, 1958) 34, 53.

[42] W. Paul and H. Steinwedel, Beta and Gamma Ray Spectroscopy, edited by K. Siegbahn (Interscience, New York, 1955).

[43] W. Bothe, Z. Naturf. 4a, 542 (1949).

[44] H. Frank, Z. Naturf. 14a, 247 (1959).

[45] H. Kulenkampf and K. Ruttiger, Z. Phys. 152, 249 (1958).

[46] H. Kanter, Annalen der Physik 20, 144 (1957).

[47] H. Seliger, Phys. Rev. 88, 408 (1952).

[48] S. Frankel, Phys. Rev. 83, 673 (1951).

[49] M. E. Rose and R. K. Osborne, Phys. Rev. 93, 1326 (1954).

[50] A. R. Edmonds, Angular Momentum in Quantum Mechanics (Princeton Univ. Press, Princeton, 1957) Chapters 5 and 7.

[51] M. G. Mayer and J. H. D. Jensen, Elementary Theory of Nuclear Shell Structure (Wiley, New York, 1955).

[52] Noya, Arima, and Horie, Pror. Theoret. Phys. (Kyoto) Supplement to No. 8, 33 (1959).

[53] N. Zeldes, Nuclear Physics 2, 1 (1956/1957).

[54] O. C. Kistner and B. M. Rustad, Phys. Rev. 114, 1329 (1959).

[55] D. L. Pursey, Phil. Mag. 42, 1193 (1951).

[56] T. Ahrens and E. Feenberg, Phys. Rev. 86, 64 (1952).

[57] Graham, Geiger, and Eastwood, Can. J. Phys. 36, 108 (1958).

Table 1. The nature of the operators in first-forbidden beta decay

(The quotation marks indicate that the "small" components of the relativistic wave functions must be used.)

Operator	Tensor Rank	Selection Rule	Lepton Angular Momentum		
			Orbital	S_e, S_ν or S_ν, S_e	Resultant
γ_5	0	$\Delta(J_i J_f 0)$	"↑"	↓↓	0
$\underset{\sim}{\sigma}\cdot\underset{\sim}{r}$	0	$\Delta(J_i J_f 0)$	↑	↓↓	0
$\underset{\sim}{\alpha}$	1	$\Delta(J_i J_f 1)$	"↑"	↓↑	↑
$\underset{\sim}{r}$	1	$\Delta(J_i J_f 1)$	↑	↑↓	↑
$\underset{\sim}{\sigma}\times\underset{\sim}{r}$	1	$\Delta(J_i J_f 1)$	↑	↑↑	↑
B_{ij}	2	$\Delta(J_i J_f 2)$	↑	↑↑	↑

Table 2. The pertinent $b_n(L,L')$'s of Bincer

$$b_o(11) = 1/2 \frac{Re}{F(Z,E)} \left\{ \left[C_A^2 M^2(\underset{\sim}{\sigma}\times\underset{\sim}{r}) + 2C_A C_V M(\underset{\sim}{\sigma}\times\underset{\sim}{r})M(i\underset{\sim}{r}) + C_V^2 M^2(i\underset{\sim}{r}) \right] K_{11} \right.$$

$$- \left[2/3\ qC_A^2\ M^2(\underset{\sim}{\sigma}\times\underset{\sim}{r}) - 2/3\ qC_V^2 M^2(i\underset{\sim}{r}) + 2C_A C_V M(\underset{\sim}{\sigma}\times\underset{\sim}{r})M(\underset{\sim}{\alpha}) \right.$$

$$\left. + 2C_V^2 M(i\underset{\sim}{r})M(\underset{\sim}{\alpha}) \right] M_{1-1}$$

$$+ \left[1/2\ C_A^2 M^2(\underset{\sim}{\sigma}\times\underset{\sim}{r}) - 2C_A C_V M(\underset{\sim}{\sigma}\times\underset{\sim}{r})M(i\underset{\sim}{r}) + 2C_V^2 M^2(i\underset{\sim}{r}) \right] K_{-2-2}$$

$$+ \left[1/6\ q^2 C_A^2 M^2(\underset{\sim}{\sigma}\times\underset{\sim}{r}) + 1/3\ q^2 C_V^2 M^2(i\underset{\sim}{r}) + 2/3\ qC_A C_V M(\underset{\sim}{\sigma}\times\underset{\sim}{r})M(\underset{\sim}{\alpha}) \right.$$

$$\left. - 2/3\ qC_V^2 M(i\underset{\sim}{r})M(\underset{\sim}{\alpha}) + C_V^2 M^2(\underset{\sim}{\alpha}) \right] K_{-1-1} \Big\}$$

$$b_0(22) = 3/8 \frac{Re}{F(Z,E)} C_A^2 M^2(iB_{ij}) \left[K_{-2-2} + 1/9\ q^2\ K_{-1-1} \right]$$

Table 2. The pertinent $b_n(L,L')$'s of Bincer (Contd)

$$b_1(11) = -1/3 \frac{Re}{F(Z,E)} \left\{ \left[C_A^2 M^2(\underset{\sim}{\sigma x r}) + 2C_V C_A M(\underset{\sim}{ir}) M(\underset{\sim}{\sigma x r}) + C_V^2 M^2(\underset{\sim}{ir}) \right] M_{11} \right.$$

$$- \left[2/3\ qC_A^2 M^2(\underset{\sim}{\sigma x r}) - 2/3\ qC_V^2 M^2(\underset{\sim}{ir}) + 2C_V C_A M(\underset{\sim}{\sigma x r}) M(\underset{\sim}{\alpha}) \right.$$

$$\left. + 2C_V^2 M(\underset{\sim}{ir}) M(\underset{\sim}{\alpha}) \right] K_{1-1}$$

$$+ \left[C_A^2 M^2(\underset{\sim}{\sigma x r}) - C_V C_A M(\underset{\sim}{ir}) M(\underset{\sim}{\sigma x r}) - 2C_V^2 M^2(\underset{\sim}{ir}) \right] M_{1-2}$$

$$- \left[1/3\ qC_A^2 M^2(\underset{\sim}{\sigma x r}) - qC_V C_A M(\underset{\sim}{ir}) M(\underset{\sim}{\sigma x r}) + 2/3\ qC_V^2 M^2(\underset{\sim}{ir}) \right.$$

$$\left. + C_A C_V M(\underset{\sim}{\sigma x r}) M(\underset{\sim}{\alpha}) - 2C_V^2 M(\underset{\sim}{ir}) M(\underset{\sim}{\alpha}) \right] K_{-1-2}$$

$$+ \left[1/4\ C_A^2 M^2(\underset{\sim}{\sigma x r}) - C_V C_A M(\underset{\sim}{ir}) M(\underset{\sim}{\sigma x r}) + C_V^2 M^2(\underset{\sim}{ir}) \right] M_{-2-2}$$

$$+ \left[1/12\ q^2 C_A^2 M^2(\underset{\sim}{\sigma x r}) - 1/3\ C_V C_A q^2 M(\underset{\sim}{ir}) M(\underset{\sim}{\sigma x r}) \right.$$

$$+ 2/3\ q\ C_A C_V M(\underset{\sim}{\sigma x r}) M(\underset{\sim}{\alpha}) - 2/3\ q\ C_V^2 M(\underset{\sim}{ir}) M(\underset{\sim}{\alpha})$$

$$\left. + C_V^2 M^2(\underset{\sim}{\alpha}) \right] M_{-1-1}$$

Table 2. The pertinent $b_n(L,L')$'s of Bincer (Contd)

$$b_1(12) = 1/2\sqrt{10}/3 \frac{Re}{F(Z,E)}\left\{\left[-C_A{}^2M(\underset{\sim}{\sigma}\times\underset{\sim}{r})M(iB_{ij})-C_AC_VM(i\underset{\sim}{r})M(iB_{ij})\right]M_{1-2}\right.$$

$$+\left[9/3\ C_A{}^2M(\underset{\sim}{\sigma}\times\underset{\sim}{r})M(iB_{ij}) - 9/3\ C_AC_VM(i\underset{\sim}{r})M(iB_{ij})\right.$$

$$\left.+ C_VC_AM(iB_{ij})M(\underset{\sim}{\alpha})\right]K_{-1-2}$$

$$+ 1/10\left[C_A{}^2M(\underset{\sim}{\sigma}\times\underset{\sim}{r})M(iB_{ij}) - 2\ C_AC_VM(i\underset{\sim}{r})M(iB_{ij})\right]M_{-2-2}$$

$$\left.- 1/18\left[q^2C_A{}^2M(\underset{\sim}{\sigma}\times\underset{\sim}{r})M(iB_{ij}) + 2q^2C_AC_VM(i\underset{\sim}{r})M(iB_{ij})\right]M_{-1-1}\right\}$$

$$b_1(22) = -3/8 \frac{Re}{F(Z,E)}\left\{C_A{}^2M^2(iB_{ij})\left[3/5\ M_{-2-2} + 1/9\ q^2\ M_{-1-1}\right]\right\}$$

Table 2. The pertinent $b_n(L,L')$'s of Bincer (Contd)

$$b_2(11) = \frac{Re}{(F(Z,E)} \left\{ \left[C_A^2 M^2(\underset{\sim}{\sigma \times r}) - C_A C_V M(\underset{\sim}{ir}) M(\underset{\sim}{\sigma \times r}) - 2C_V^2 M^2(\underset{\sim}{ir}) \right] K_{1-2} \right.$$

$$- \left[1/3\ qC_A^2 M^2(\underset{\sim}{\sigma \times r}) - qC_A C_V M(\underset{\sim}{ir}) M(\underset{\sim}{\sigma \times r})\ M_{-1-2} \right.$$

$$\left. + 2/3\ qC_V^2 M^2(\underset{\sim}{ir}) + C_A C_V M(\underset{\sim}{\sigma \times r}) M(\underset{\sim}{\alpha}) - 2C_V^2 M(\underset{\sim}{ir}) M(\underset{\sim}{\alpha}) \right]$$

$$\left. - \left[1/4\ C_A^2 M^2(\underset{\sim}{\sigma \times r}) - C_A C_V M(\underset{\sim}{ir}) M(\underset{\sim}{\sigma \times r}) + C_V^2 M^2(\underset{\sim}{ir}) \right] K_{-2-2} \right\}$$

$$b_2(12) = \sqrt{3/10}\ \frac{Re}{F(Z,E)} \left\{ \left[C_A^2 M(\underset{\sim}{\sigma \times r}) M(iB_{ij}) + C_A C_V M(\underset{\sim}{ir}) M(iB_{ij}) \right] K_{1-2} \right.$$

$$- \left[1/3\ qC_A^2 M(\underset{\sim}{\sigma \times r}) M(iB_{ij}) - 1/3\ qC_A C_V M(\underset{\sim}{ir}) M(iB_{ij}) \right.$$

$$\left. + C_A C_V M(\underset{\sim}{\alpha}) M(iB_{ij}) \right] M_{-1-2}$$

$$\left. + \left[1/2\ C_A^2 M(\underset{\sim}{\sigma \times r}) M(iB_{ij}) - C_A C_V M(\underset{\sim}{ir}) M(iB_{ij}) \right] K_{-2-2} \right\}$$

$$b_2(22) = 21/40\ \frac{Re}{F(Z,E)}\ C_A^2 M^2(iB_{ij})\ K_{-2-2}$$

Table 3. The approximate magnitude of the $b_n(L,L')$'s

Parameter	Highest power of ξ	Relative Magnitude
$b_0(11)$	2	100
$b_0(22)$	0	1
$b_1(11)$	2	100
$b_1(12)$	1	10
$b_1(22)$	0	1
$b_2(11)$	1	10
$b_2(12)$	1	10
$b_2(22)$	0	1
$b_3(22)$	0	1

Table 4. Matrix Elements in Spherical Tensor Form

$$M(i\underset{\sim}{r}) = \sqrt{\frac{4\pi}{3(2J_i+1)}}\,(J_f L_f S_f||T_{11}(1,\underset{\sim}{r})||J_i L_i S_i)$$

$$M(\underset{\sim}{\sigma}\times\underset{\sim}{r}) = -\sqrt{\frac{8\pi}{3(2J_i+1)}}\,(J_f L_f S_f||T_{11}(\underset{\sim}{\sigma},\underset{\sim}{r})||J_i L_i S_i)$$

$$M(iB_{ij}) = \mp\sqrt{\frac{16\pi}{3(2J_i+1)}}\,(J_f L_f S_f||T_{21}(\underset{\sim}{\sigma},\underset{\sim}{r})||J_i L_i S_i)$$

$$M(\underset{\sim}{\alpha}) = +\sqrt{\frac{4\pi}{2J_i+1}}\,(J_f L_f S_f||T_{10}(\frac{i\Delta}{M},\underset{\sim}{r})||J_i L_i S_i)$$

Table 5. $M(\underset{\sim}{\alpha})/M(\underset{\sim}{\sigma} \times \underset{\sim}{r})$ for three evaluations

Wave Function Employed	$\frac{M(\underset{\sim}{\alpha})}{M(\underset{\sim}{\sigma} \times \underset{\sim}{r})}$
"Exact", $R \doteq 1.3\ A^{1/3}\ 10^{-13}$ cm	-29.4 ± 1.4
"Exact", $R \doteq 1.2\ A^{1/3}\ 10^{-13}$ cm	-29.5 ± 2.3
"Approximate", $R = 1.3\ A^{1/3}\ 10^{-13}$ cm	-36.6 ± 1.0

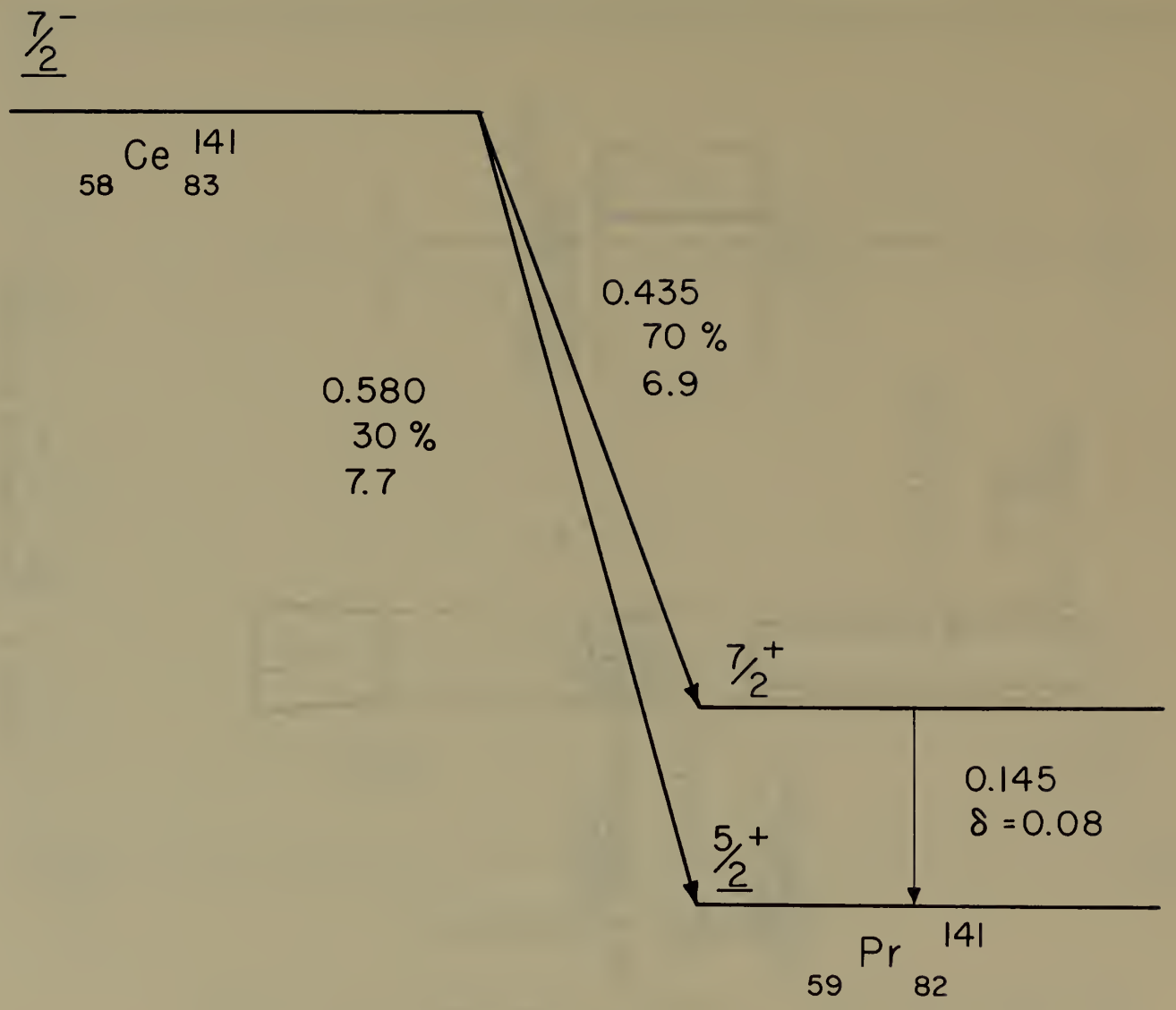

Figure 1. Ce^{141} decay scheme.

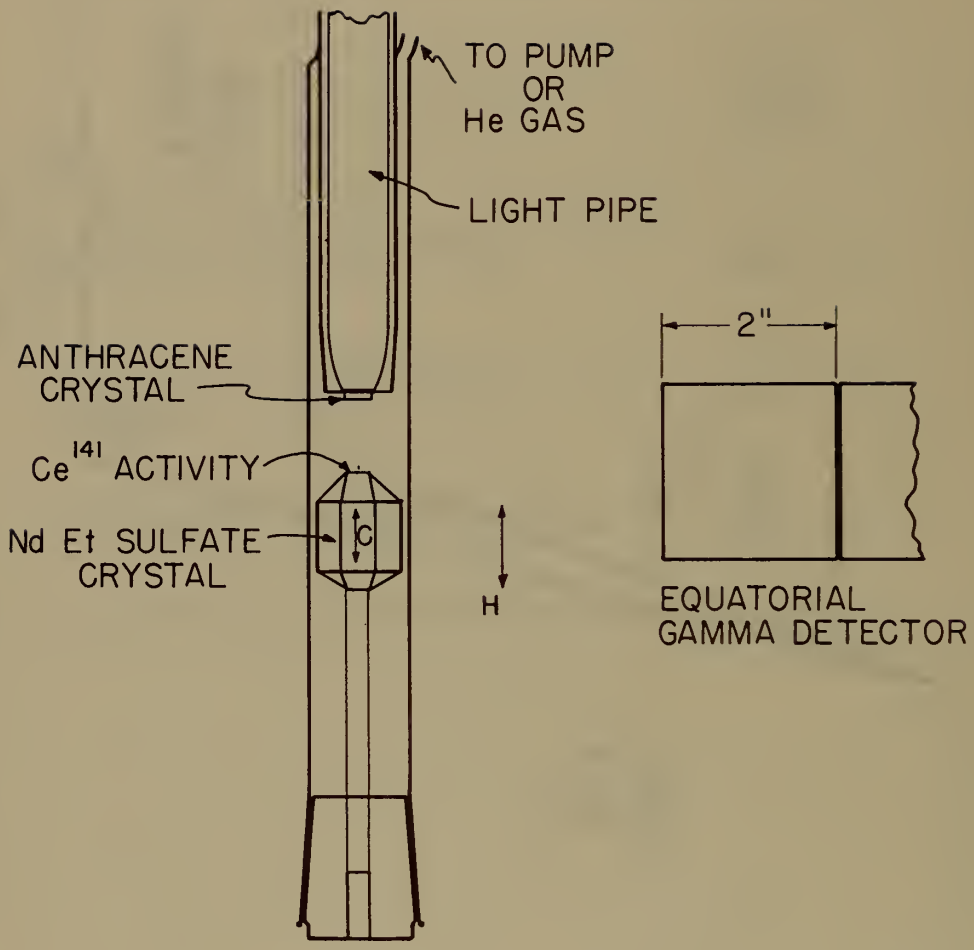

Figure 2. Experimental apparatus.

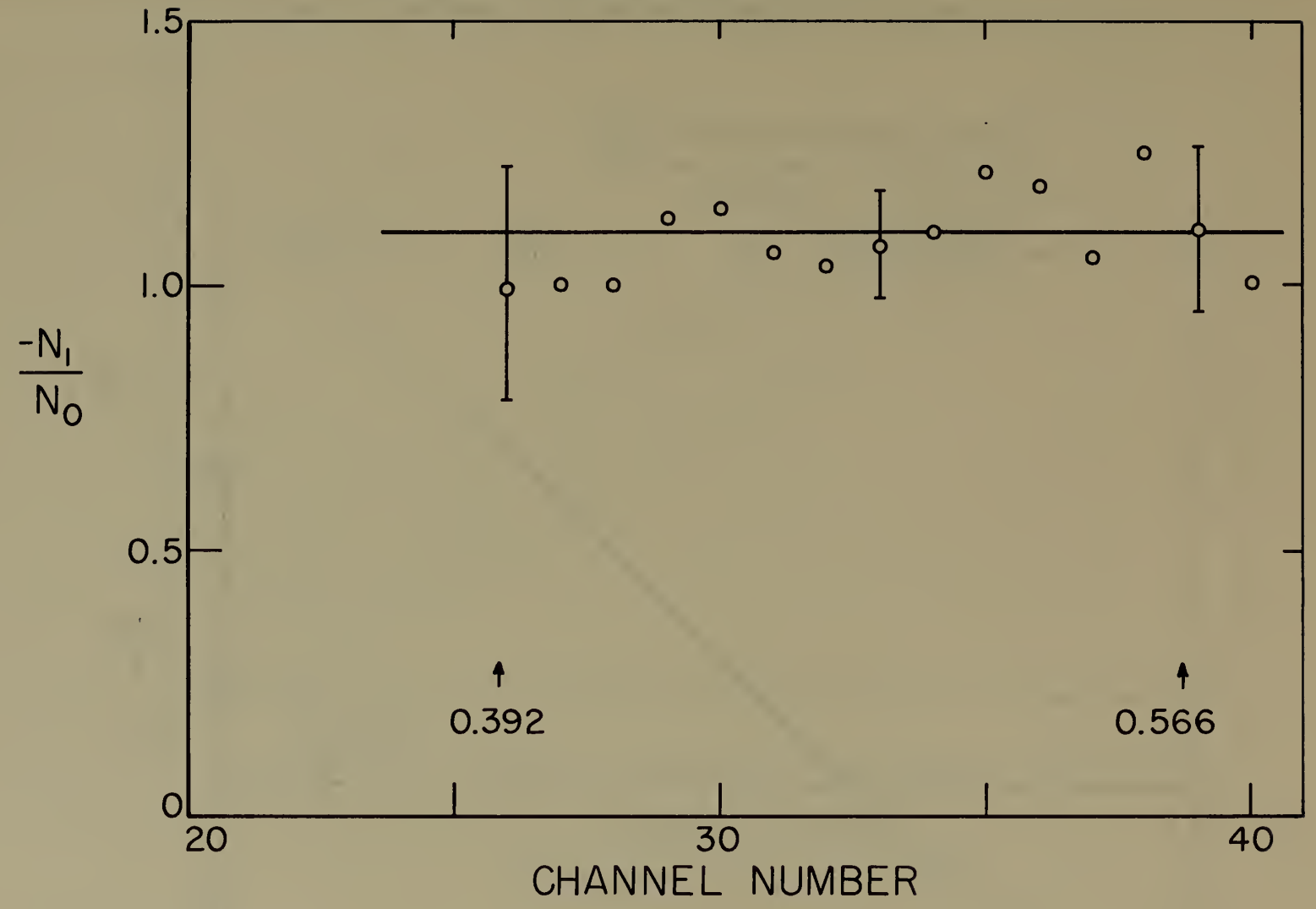

Figure 3. The experimental variation of the quantity N_1/N_0 with nominal beta energy.

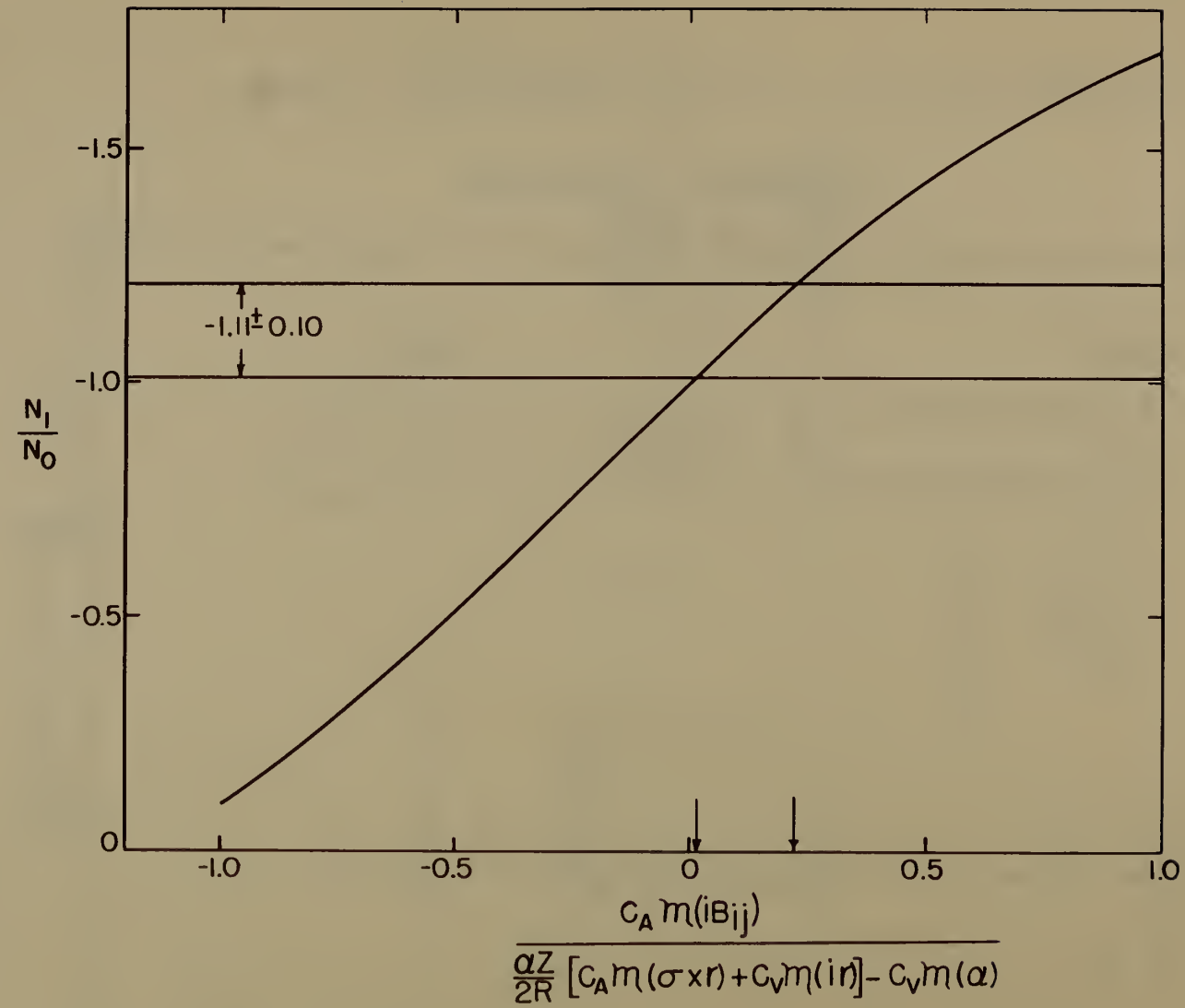

Figure 4. The quantity N_1/N_0 as a function of tensor rank two admixture, in an approximate analysis.

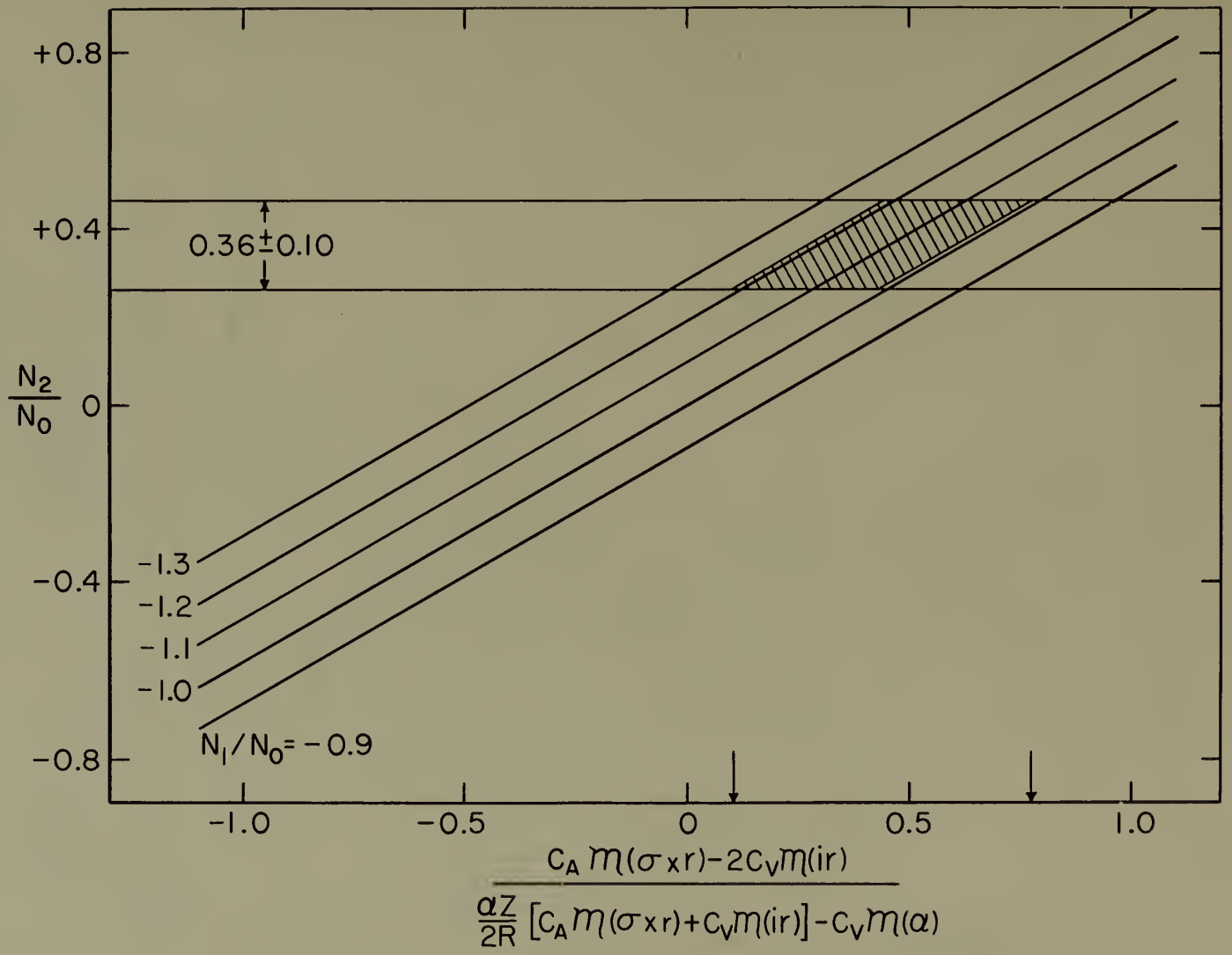

Figure 5. The quantity N_2/N_0 as a function of tensor rank one parameters, in an approximate analysis. The range of values allowed by experiment is indicated on the curve.

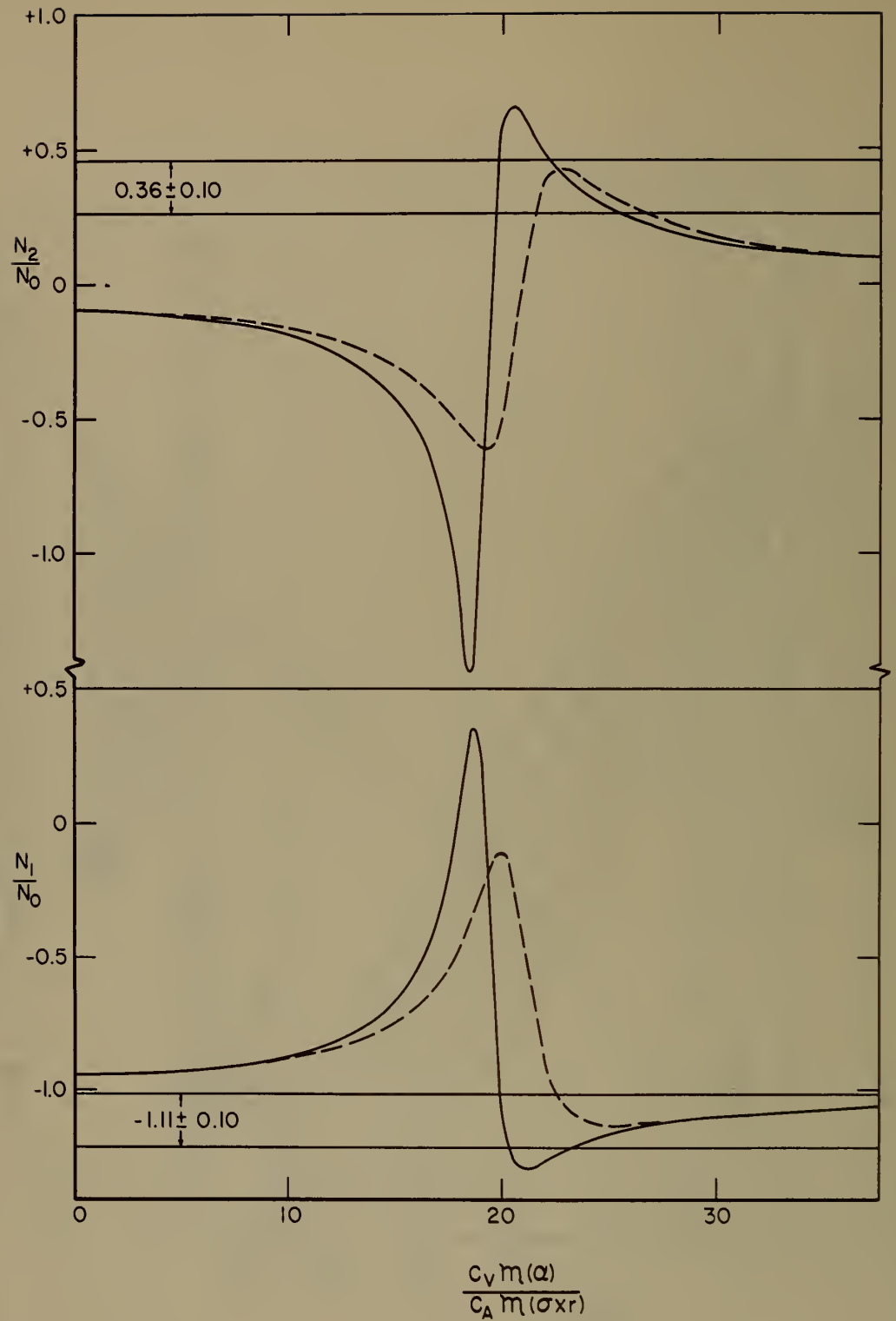

Figure 6. A comparison of the experimental coefficients with the predictions of an "exact" analysis in which the ratio $M(\alpha)/M(\sigma x r)$ is the only free parameter. The solid curve is for a nuclear radius of $1.3 \times A^{1/3} \times 10^{-13}$ cm; the dotted line is for a radius 8% smaller.

U. S. DEPARTMENT OF COMMERCE
Luther H. Hodges, *Secretary*

NATIONAL BUREAU OF STANDARDS
A. V. Astin, *Director*

THE NATIONAL BUREAU OF STANDARDS

The scope of activities of the National Bureau of Standards at its major laboratories in Washington, D.C., and Boulder, Colorado, is suggested in the following listing of the divisions and sections engaged in technical work. In general, each section carries out specialized research, development, and engineering in the field indicated by its title. A brief description of the activities, and of the resultant publications, appears on the inside of the front cover.

WASHINGTON, D.C.

Electricity. Resistance and Reactance. Electrochemistry. Electrical Instruments. Magnetic Measurements. Dielectrics.

Metrology. Photometry and Colorimetry. Refractometry. Photographic Research. Length. Engineering Metrology. Mass and Scale. Volumetry and Densimetry.

Heat. Temperature Physics. Heat Measurements. Cryogenic Physics. Equation of State. Statistical Physics.

Radiation Physics. X-ray. Radioactivity. Radiation Theory. High Energy Radiation. Radiological Equipment. Nucleonic Instrumentation. Neutron Physics.

Analytical and Inorganic Chemistry. Pure Substances. Spectrochemistry. Solution Chemistry. Standard Reference Materials. Applied Analytical Research.

Mechanics. Sound. Pressure and Vacuum. Fluid Mechanics. Engineering Mechanics. Rheology. Combustion Controls.

Organic and Fibrous Materials. Rubber. Textiles. Paper. Leather. Testing and Specifications. Polymer Structure. Plastics. Dental Research.

Metallurgy. Thermal Metallurgy. Chemical Metallurgy. Mechanical Metallurgy. Corrosion. Metal Physics. Electrolysis and Metal Deposition.

Mineral Products. Engineering Ceramics. Glass. Refractories. Enameled Metals. Crystal Growth. Physical Properties. Constitution and Microstructure.

Building Research. Structural Engineering. Fire Research. Mechanical Systems. Organic Building Materials. Codes and Safety Standards. Heat Transfer. Inorganic Building Materials.

Applied Mathematics. Numerical Analysis. Computation. Statistical Engineering. Mathematical Physics. Operations Research.

Data Processing Systems. Components and Techniques. Digital Circuitry. Digital Systems. Analog Systems. Applications Engineering.

Atomic Physics. Spectroscopy. Infrared Spectroscopy. Solid State Physics. Electron Physics. Atomic Physics.

Instrumentation. Engineering Electronics. Electron Devices. Electronic Instrumentation. Mechanical Instruments. Basic Instrumentation.

Physical Chemistry. Thermochemistry. Surface Chemistry. Organic Chemistry. Molecular Spectroscopy. Molecular Kinetics. Mass Spectrometry.

Office of Weights and Measures.

BOULDER, COLO.

Cryogenic Engineering. Cryogenic Equipment. Cryogenic Processes. Properties of Materials. Cryogenic Technical Services.

Ionosphere Research and Propagation. Low Frequency and Very Low Frequency Research. Ionosphere Research. Prediction Services. Sun-Earth Relationships. Field Engineering. Radio Warning Services.

Radio Propagation Engineering. Data Reduction Instrumentation. Radio Noise. Tropospheric Measurements. Tropospheric Analysis. Propagation-Terrain Effects. Radio-Meteorology. Lower Atmosphere Physics.

Radio Standards. High Frequency Electrical Standards. Radio Broadcast Service. Radio and Microwave Materials. Atomic Frequency and Time Interval Standards. Electronic Calibration Center. Millimeter-Wave Research. Microwave Circuit Standards.

Radio Systems. High Frequency and Very High Frequency Research. Modulation Research. Antenna Research. Navigation Systems.

Upper Atmosphere and Space Physics. Upper Atmosphere and Plasma Physics. Ionosphere and Exosphere Scatter. Airglow and Aurora. Ionospheric Radio Astronomy.


NBS